Theoretical Computer Science 405 (2008) 41–49

Contents lists available at ScienceDirect

Theoretical Computer Science

journal homepage: www.elsevier.com/locate/tcs

Modeling time and topology for animation and visualization with examples on parametric geometry

K.E. Jordan [a], Lance E. Miller [b], E.L.F. Moore [b], T.J. Peters [b,*], Alexander Russell [b]

[a] *IBM Corporation, One Rogers Street, Cambridge, MA 02142, USA*

[b] *Department of Computer Science, University of Connecticut, Storrs, CT 06269-2155, USA*

ARTICLE INFO

Keywords:
Ambient isotopy
Computational topology
Temporal aliasing
Animation
Visualization
Curve approximation

ABSTRACT

The art of animation relies upon modeling objects that change over time. A sequence of static images is displayed to produce an illusion of motion. Even for simple cases, a careful analysis exposes that formal topological guarantees are often lacking. This absence of rigor can result in subtle, but significant, topological flaws. A new modeling approach is proposed to integrate topological rigor with a continuous model of time. Examples will be given for Bézier curves, while indicating extensions to a richer class of parametric curves and surfaces. Applications to scientific visualization for molecular modeling are discussed. Prototype animations are available for viewing over the web.

© 2008 Elsevier B.V. All rights reserved.

1. Introduction: Analysis of topological flaws in time models

The animation paradigm described in the abstract was established by human animators and persists in contemporary computer animation, where the individual static images are known as *frames* and distinct geometric models are created for each frame. Unwanted artifacts are possible [31].

For example, in creating a protein-enzyme simulation, the actual dynamics of the underlying physical system may naturally avoid topological changes (such as fracture of a twisting DNA strand), but the underlying algorithms are not designed to ensure the global topology of the perturbing model. As the objects can be geometrically complex, it becomes impractical and unreliable for humans to attempt to visually detect any unwanted artifacts. The dominant approach today is to post-process the geometry in each frame by testing for self-intersections as opposed to modeling the continuous motion [30].

A careful analysis of this approach exposes two main difficulties:

(1) Any self-intersection *between* frames would remain undetected.
(2) Algorithms for detecting self-intersections are compute intensive.

The first difficulty is inherent in the approach of only inspecting static images. That approach tacitly assumes that the time differences between each frame are sufficiently small to preclude self-intersections between frames. However, such self-intersections can occur and disappear instantaneously, as illustrated in Fig. 1. The drawings of Fig. 1 have a simplified schematic of an instantaneous, pernicious topological change. The topology of the unknot (on the left) changes *instantaneously* upon the appearance of the self-intersection shown at the top of the middle image. Subsequently, further topological change results in a trefoil knot.

* Corresponding author.
E-mail addresses: kjordan@us.ibm.com (K.E. Jordan), lance.e.miller@gmail.com (L.E. Miller), tpeters@cse.uconn.edu, tpeters@engr.uconn.edu (T.J. Peters), acr@cse.uconn.edu (A. Russell).

0304-3975/$ – see front matter © 2008 Elsevier B.V. All rights reserved.
doi:10.1016/j.tcs.2008.06.023

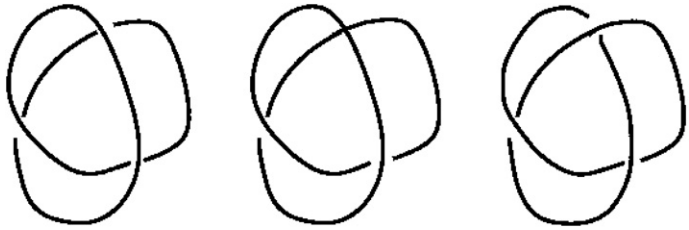

Fig. 1. Self-intersection precedes knot change.

The topological emphasis presented here will prevent even these instantaneous temporal artifacts. This new computational approach to modeling time for animation and dynamic visualization relies upon Lemma 3.1 proven here to permit the synthesis of several results into a new methodology.

2. Related work

The proposed approach focuses upon topological equivalence over the time variable used in simulations. Preventing unwanted new self-intersections is important to avoid temporal aliasing in animation [21]. Progress in computational topology invariants has advanced greatly through research on biological applications [4,5,17,18]. The role of knot characteristics has been prominent for molecular modeling [47]. The classical tubular neighborhoods are fundamental for isotopy [26] equivalence, as invoked in a contemporary algorithm for a piecewise liner (PL) ambient isotopic approximant to a parametric curve [32]. Surface approximations based upon ϵ-nets and Delaunay triangulations have also appeared [14].

A seminal work on the integration of graphics for simulation [48] emphasized efficient algorithms for culling, scaling and clipping of geometry when no topological changes were expected. A focus on polylines or polyhedra [16,20,22,25] or other specialized shapes [3,40] has been motivated by performance concerns. Visualization and graphics of massive data sets have been studied [3,15,23–25,28] as well as applications for the life sciences [29,44].

The current authors have contributed to the emphasis upon algorithms for isotopic equivalence between a parametric curve and its piecewise liner (PL) approximant [33,34,36,37]. Algorithms for preservation of topological form during perturbation of vertices and control points, for polyhedra and splines, respectively, have given practically computable limits on the distance these points can be perturbed [7–9].

3. Isotopy for Bézier curves

A curve will be the image of a continuous function $\mathbf{c} : [0, 1] \to \mathbb{R}^3$. These curves are necessarily compact. These curves can be open or closed and have self-intersections. Since the focus will be on ambient isotopic equivalence, that definition is given.

Definition 3.1. Let X and Y be two subspaces of $\mathbb{R}^n$. A continuous function

$$H : \mathbb{R}^n \times [0, 1] \to \mathbb{R}^n$$

is an **ambient isotopy** between X and Y if H satisfies the following:

(1) $H(\cdot, 0)$ is the identity,
(2) $H(X, 1) = Y$, and
(3) $\forall t \in [0, 1]$, $H(\cdot, t)$ is a homeomorphism from $\mathbb{R}^n$ onto $\mathbb{R}^n$.

The sets X and Y are then said to be **ambient isotopic**.

3.1. Curves for graphics

For the curves used in graphics, animation and visualization, it is often assumed that they are non-self-intersecting. Many of the curves used are splines, and the special case of a Bézier curve [42] is defined, below.

Definition 3.2. A **Bézier curve** is defined by $\mathbf{b} : [0, 1] \to \mathbb{R}^n$ for $n = 1, 2, \ldots$ as

$$\mathbf{b}(u) = \sum_{i=0}^{n} B_{i,n}(u)\mathbf{P}_i,$$

where

$$B_{i,n}(u) = \frac{n!}{i!(n-i)!} u^i (1-u)^{n-i},$$

where the $B_{i,n}$ are the classical n-th degree Bernstein polynomials and the $\mathbf{P}_i$ are known as the **control points**.

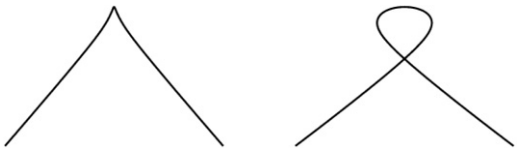

Fig. 2. Topological change by perturbed control points.

A curve of Definition 3.2 is known as single segment curve but such single curves are joined into composite curves, with common usage being to also refer to these resultant curves as Bézeier curves and the points in $\mathbb{R}^n$ where the single segments Bézier curves are joined are called junction points [19]. While any single segment Bézier is C^∞, when considering a composite Bézier curve, the degree of differentiability is determined by differentiability at the junction points.

Even if the original curve is non-self-intersecting, when the geometry changes dynamically during animation or visualization, it is possible to introduce new self-intersections. This phenomenon is depicted for a planar Bézier curve in Fig. 2, where the transition from left to right is achieved by perturbation of the control points. The left image has no self-intersections. However, continuous movement of the control points can cause the curve to instantaneously pass through a cusp [42], while further movement of these control points can cause self-intersection, as shown in the right image.

3.2. Perturbation limits and isotopy

Previous work [8] presented tractable computational limits on the perturbation of control points to preclude introduction of self-intersections for Bézier curves and surfaces. For ease of exposition, the summary presented here will only consider the case of a single segment Bézier curve, denoted as **b**. This captures the essence and the additional subtleties necessary to extend the results here to composite rational Bézier curves follow from the previous work [8].

Presenting that previous work relies upon the definition of the finite sequence **q** defined on the control points of **b** as

$$\mathbf{q} = \{\mathbf{P}_1 - \mathbf{P}_0, \ldots, \mathbf{P}_n - \mathbf{P}_{n-1}\}.$$

Let $\mathrm{conv}(\mathbf{q})$ denote the convex hull of **q** and let $d^*(\mathbf{q}) = d_E(\mathbf{0}, \mathrm{conv}(\mathbf{q}))$, where **0** is the origin and d_E denotes the Euclidean distance between a point and a polyhedron. The first result used here is the following:

Proposition 3.1 (*[8]*). *A sufficient condition for non-self-intersection of the Bézier curve* **b** *is that* $d^*(\mathbf{q}) > 0$.

While this gives a tractable criterion for determining non-self-intersection of a static Bézier curve, it was also generalized to limit how far the control points could be perturbed without introducing self-intersections. For each $i = 0, 1, \ldots, n$, let $\delta\mathbf{P}_i$ represent the perturbation of each control point $\mathbf{P}_i$ and let $\delta\mathbf{q}$ be given by

$$\delta\mathbf{q} = \{\delta\mathbf{P}_0, \delta\mathbf{P}_1, \ldots, \delta\mathbf{P}_n\}.$$

Let $\|\delta\mathbf{q}\| = \max\{\|\delta\mathbf{P}_i\| : i = 0, 1, \ldots, n\}$, with the Euclidean norm on each $\delta\mathbf{P}_i$. The perturbation result used here is the following:

Proposition 3.2 (*[8]*). *If* $d^*(\mathbf{q}) > 0$ *and* $\|\delta\mathbf{q}\| < d^*(\mathbf{q})$, *then the perturbed curve remains non-self-intersecting.*

While this perturbation result only treats a single perturbed curve, it should be clear that if the control points are linearly perturbed to their new positions, then any Bézier curve defined by intermediate positions of those linearly perturbing points is also non-self-intersecting. Linear perturbations of control points are used frequently in graphics, animation and visualization. It is easy to see that each linear perturbation of the control points is a homotopy, which can be extended to an isotopy under the following conditions.

Lemma 3.1. *Let* **c** *be a non-self-intersecting* C^2 *parametric curve,*

$$\mathbf{c} : [0, 1] \to \mathbb{R}^n.$$

Let F be a homotopy of **c** *given by* $F : [0, 1] \times [0, 1] \to \mathbb{R}^n$ *such that*

$$F(s, t) = \mathbf{c}(s),$$

and such that each homotopic image of **c** *is non-self-intersecting, then there exists an ambient isotopy,* $H : \mathbb{R}^n \times [0, 1] \to \mathbb{R}^n$, *such that, if* $s \in [0, 1]$, *then*

$$H(F(s; 0); t) = F(s; t).$$

Proof. The C^2 hypothesis and the compactness of **c** ensure that **c** has a PL approximation [32], specifically **c** is *not* a wild arc [27]. Since the domain of **c** is compact and each homotopic image is non-self-intersecting, then $\forall t \in [0, 1]$ the map given by $H(F(s; 0); t) = F(s; t)$ is a homeomorphism. It should also be clear that the union of all the images given by $H(F(s; 0); t) = F(s; t)$ over all $t \in [0, 1]$ can be contained within a compact polyhedron. Then a standard argument can be made for the existence of an ambient isotopy with compact support [7]. □

3.3. Animating a curve

Proposition 3.2 and Lemma 3.1 suffice to exhibit families of Bézier curves that are ambient isotopic within the indicated perturbation limits. If the animation requires perturbation limits that exceed these sufficient conditions, then the perturbation can be refined into smaller steps and each one analyzed separately. So, further attention here will be restricted to a given time interval $[0, T]$ corresponding to a perturbation less than $d^*(\mathbf{q})$.

For any $t \in [0, T]$, the partial perturbation at time t will be ambient isotopic to $\mathbf{b}$, where both $\mathbf{b}$ and its perturbation are Bézier curves. The paradigms for animation and dynamic visualization still require a choice of finitely many times $\{t_0, t_1, \ldots, t_m\}$, (with $t_0 = 0$ and each $t_j \in [0, T]$) so displaying these $m + 1$ images at a sufficiently high frequency will be perceived as motion. For any such t_j, the corresponding Bézier curve will be ambient isotopic to the original curve.

However, graphics subsystems typically rely upon piecewise linear (PL) approximations of curves in order to render them. It is well known that PL approximation need not preserve the isotopy class of the original curve [6]. Hence, it remains to determine how ambient isotopic PL approximations can be integrated into this scheme. The first step, of course, is to find an appropriate approximation of $\mathbf{b}$.

Previous work [9] has given sufficient conditions for topological complexes of surface patches to be ambient isotopic under perturbations of control points, but this work did not provide ambient isotopic PL approximations, which is presented for a class of curves in the next section.

4. Tubular neighborhoods: Theory & practice

The techniques used in this paper are standard within differential topology regarding tubular neighborhoods and the extension of isotopies to ambient isotopies [26,27,43]. Much of the following material can be seen as applications of that theory. However, as is common in the transition of theoretical mathematics to practical algorithms, the level of abstraction changes. This section explicates details of the transition of abstract existence results into efficient, constructive algorithms. The crucial computation is the radius of a tubular neighborhood. This exposition will proceed with construction of a tubular neighborhood about a curve, but the construction is similar for higher order manifolds [1,2,6,41,45,46].

The curves are assumed to be C^2. Two published algorithms for creating ambient isotopic PL approximation of parametric curves are considered. Both techniques [32,39] create a tubular neighborhood of the curve as a containment for the PL approximation. Similar techniques are being used for both new theoretical findings and improved visualization of knots [12, 13].

Let r denote the radius of this tubular neighborhood. Computation of this radius depends upon two other values. The first is the maximum value of curvature, denoted as κ_M. This maximum exists because of the continuity and compactness properties of the curves considered. Algorithms for this computation are standard [42]. The other value is known as the minimum separation distance (*MSD*), which is defined by taking the minimum over all pairs of points whose normals are collinear. Algorithms for computing *MSD* are available [32–34] and the continuity and compactness criteria ensure that $MSD > 0$, except for the trivial case of a line segment. Then, the radius r is defined as

$$r = \min(1/\kappa_M, (1/2)MSD). \tag{1}$$

The paper [32] uses this definition of r for creation of ambient isotopic PL approximations for a rich class of spline curves that properly includes Bézier curves. For a curve $\mathbf{c}$, its PL approximation is defined by a finite sequence of points in $[0, 1]$

$$0 = t_0 < t_1 < \cdots < t_k = 1,$$

to give the PL approximation, $pl(\mathbf{c})$ formed by the polyline formed over the set of vertices, V, ordered as

$$V = \{\mathbf{c}(t_0), \mathbf{c}(t_1), \ldots, \mathbf{c}(t_k)\}. \tag{2}$$

Other PL approximations mentioned later create sets similar to V. For the isotopy constructed between $\mathbf{c}$ and $pl(\mathbf{c})$, all the vertices of V are fixed points.

5. Perturbing PL approximations of Bézier curves

Let $\mathbf{b}$ denote a non-self-intersecting Bézier curve, such that $d^*(\mathbf{q}) > 0$ and $\|\delta\mathbf{q}\| < d^*(\mathbf{q})$. Compute r of Eq. (1) for $\mathbf{b}$ and choose $\epsilon > 0$ (to avoid the trivial case of a line segment) such that $r > \epsilon > 0$ and create a PL approximation of $\mathbf{b}$ to fit inside the tubular neighborhood of radius r, where the vertices are chosen as in V of Eq. (2).

Combining the previous discussions from Section 3.2 and 4, yields the following result.

Proposition 5.1. *If $\mathbf{b}$ is a C^3 Bézier curve, with $d^*(\mathbf{q}) > 0$ and $\|\delta\mathbf{q}\| < d^*(\mathbf{q})$, then these perturbations of $\mathbf{b}$ are ambient isotopic and there exists a PL ambient isotopic approximation of $\mathbf{b}$ within the tubular neighborhood of radius r.*

Now consider the times $\{t_0, t_1, \ldots, t_m\}$ indicated in Section 3.3. The original curve $\mathbf{b}$ occurs at time t_0. Let $\mathbf{b}_j$ denote the perturbed Bézier curve at time t_j, with $\mathbf{b} = \mathbf{b}_0$. In order to create an ambient isotopic approximation of each $\mathbf{b}_j$ by use of the preceding results, one would need to verify the hypothesis that each $\mathbf{b}_j$ was either C^2 or C^3, depending upon the approximation technique used. This would permit an arbitrarily close ambient isotopic PL approximation to each $\mathbf{b}_j$. However, the previous discussion regarding Fig. 2 indicates that perturbation of the control points can change the differentiability class. An obvious option would be constraints to preserve the needed differentiability, but this raises questions in differential topology that are beyond the scope of the present paper.

However, Lemma 3.1 provides an alternative in absence of the verification of the needed differentiability. Namely, let $pl(\mathbf{b}_0)$ denote any PL approximation of $\mathbf{b}_0$. Published perturbation limits to prevent self-intersections of PL curves [7] rely on defining a parameter ν as the minimum of all distances between disjoint pairs of vertices and segments in the PL curve. Once $pl(\mathbf{b}_0)$ is known, the determination of its ν is a trivial computation. Proposition 5.1 can be now rephrased as follows

Proposition 5.2. *If* $\mathbf{b}$ *is a* C^3 *Bézier curve, with* $d^*(\mathbf{q}) > 0$ *and* $\|\delta\mathbf{q}\| < d^*(\mathbf{q})$*, and if* $\mathbf{b}$ *has a PL ambient isotopic approximation with* $\nu < \|\delta\mathbf{q}\|$*, then these perturbations of* $\mathbf{b}$ *are ambient isotopic and each has an ambient isotopic PL approximation given as the corresponding perturbation of* $pl(\mathbf{b}_0)$*.*

The crucial theoretical observation is that attending first to the preservation of topology leads to guarantees for any time chosen within the interval. Only after that were specific time values chosen to obtain approximations. This avoids the problem of first discretizing the time, only to find that one could have missed a crucial topological change (or even worse, to be oblivious to that pernicious error). The importance of this to molecular simulations [38] is discussed in Section 7. It is noted that similar perturbation bounds are known for higher dimensional spline manifold geometry [8,9], leading to immediate generalizations of the work presented in this section.

6. Creating *V* and general parametric curves

Previous methods for isotopic approximation of curves [32] did not explicate the creation of the set V of approximating points of Eq. (2) and were restricted to NURBS curves. This section provides an explicit method for creating V — moreover, the method is adaptive to curvature, meaning that fewer approximating points are chosen in segments of low curvature versus than for high curvature. Also, the family of curves extends beyond NURBS curves. A similar result for approximating surfaces was done concurrently [14], but the method here produces new quantitative bounds based upon a more direct proof for the simpler case of curves.

In Section 5, perturbations bounds to maintain isotopy were available directly on the original control points of the Bézier curves. However, in the more general parametric geometry context, the convenience of control points will not typically be available. But, for many practical applications, once the PL approximation is available, one only needs to know perturbation bounds on those vertices, but these are known [7] and have already been used in practical animation algorithms [21].

The approximation techniques of this section are adaptive to curvature so that the number of approximating segments is asymptotically optimal as the bound on the approximation error goes to zero. Since performance of the graphics operations is optimized by limiting the number of segments to be displayed, these refinements are of practical interest.

An adaptive, piecewise linear approximation of the curve c is given relative to its *bending energy*, which is denoted as $\beta(c)$ and defined here as

$$\beta(c) = \int_0^1 \|c''(s)\| \, \mathrm{d}s. \tag{3}$$

Throughout this section, the curve c will be assumed to be non-self-intersecting.

The techniques presented here *not only* provide rigorous error bounds on the Hausdorff distance between c and its PL approximant, *but also* establish bounds upon tangency differences between the approximant and c.

Fix $\epsilon > 0$. For any $t \in [0, 1]$, it follows from Taylor's Theorem, with the Cauchy form for the remainder [11], that $h(t)$ can be chosen such that

$$\int_t^{t+h(t)} \|c''(u)\| \, \mathrm{d}u = \epsilon. \tag{4}$$

A family of cylinders will be inductively defined to be represented by subintervals of $[0, 1]$ such that the following holds:

(i) Each point on the curve will lie in the interior of at least one cylinder.
(ii) Each point in $[0, 1]$ is contained in no more than two of the subintervals.
(iii) Within each cylinder the error bound between the curve and its approximation will be no more than ϵ.

Notation. Let $N(\epsilon, c)$ be the number of cylinders inductively defined with error tolerance ϵ on curve c. Let $t_0 = 0$. Then define $t_1 \leq 1$ be such that

$$\int_{t_0}^{t_1} \|c''(z)\| \mathrm{d}z = \epsilon.$$

Here, t_1 plays the role of the notation $t + h(t)$ previously used in Eq. (4). For $i \geq 1$, we similarly define t_{i+1} inductively, so that for $t_i < t_{i+1}$, each integral $\int_{t_i}^{t_{i+1}} |c''(z)| \mathrm{d}z = \epsilon$ and

$$\sum_{i=0}^{N(\epsilon,c)-1} \int_{t_i}^{t_{i+1}} |c''(z)| \mathrm{d}z \leq \int_0^1 |c''(z)| \mathrm{d}z < \infty,$$

so this procedure will terminate.

A minor subtlety arises in choosing t_{n+1}. This is easily resolved. Observe that $\int_{t_n}^1 |c''(z)| \mathrm{d}z \leq \epsilon$ and first assume that c is closed, so that t_{n+1} can be chosen to be 1. If c is not closed, then the last cylinder should be taken to extend slightly past the end point.

The PL approximation of c is then given by the polyline joining the points

$$\{c(t_0), c(t_1), \ldots, c(t_n), c(t_{n+1})\}$$

in the order given by their indices.

There is an asymptotic upper bound for the number of cylinders used in terms of the error bound and the global curvature:

Proposition 6.1. *For the family described there are at most $O(\int \|c''(u)\| \mathrm{d}u/\epsilon)$ many cylinders in the family.*

Proof. Observe that

$$\sum_{i=0}^{N(\epsilon,c)-1} \int_{t_i}^{t_{i+1}} \|c''(u)\| \mathrm{d}u = \int_0^1 \|c''(u)\| \mathrm{d}u$$

by condition (ii). Also, by construction each summand is at most ϵ, so

$$N(\epsilon, c) \leq (1/\epsilon) \int_0^1 \|c''(u)\| \mathrm{d}u. \quad \square$$

However, this is a coarse upper bound, due to the assumption here that h is just less than 1, when h will often be much smaller. As a quick demonstration of this, assume that c has constant second derivative. From the analysis above, there exists an error bound of $h \int_t^{t+h} \|c''(u)\| \mathrm{d}u$. Suppose $\|c''(u)\|$ is constant, with this constant denoted as K. If $K = 0$ then this is the trivial case of a straight line which can be contained within one cylinder. If $K \neq 0$ then there exists an error bound $h^2 \cdot K$. Evidently, the choice can be $h = \sqrt{\epsilon/K}$ so that $N(\epsilon, c) \cdot h = 1$ and $N(\epsilon, c)\sqrt{\epsilon} = \sqrt{K}$. This discussion is a proof of the following lemma.

Lemma 6.1. *If $\|c''(t)\| \equiv K$ is constant, then $\sqrt{\epsilon} \cdot N(\epsilon, c) = O(1)\sqrt{K}$.*

This is suggestive of a sharper bound for $N(\epsilon, c)$.

Lemma 6.2. *If c is C^3 and if there exists $\alpha > 0$ such that $\|c''(t)\| \geq \alpha > 0$ for all t, then*

$$\lim_{\epsilon \to 0} \sqrt{\epsilon} \cdot N(\epsilon, c) = O(1) \int_0^1 \sqrt{\|c''(u)\|} \mathrm{d}u.$$

Proof. Let $\gamma > 0$ be an error estimate. Let $M_3 = \max\{\|c'''(u)\|\}$ and define $\nu = (1/\sqrt{2}) \int_0^1 \sqrt{\|c''(u)\|} \mathrm{d}u$. Choose a mesh $\eta > 0$ of an even subdivision $\{t_i\}$ of the interval in order to approximate ν by Riemann sums and $\epsilon > 0$, so that the lengths of the cylinders lie within the η-intervals. Specifically choose η_1 such that the Riemann sum

$$\left| \sum_{i=0}^{\eta_1^{-1}} \frac{\eta_1 \sqrt{\|c''(t_i)\|(1 + \frac{\eta_1 M_3}{\alpha})}}{\sqrt{2}} - \nu \right| \leq \frac{\gamma}{2},$$

and choose $\eta < \min\{\eta_1, (\alpha/M_3)\}$. Also choose

$$\epsilon < \frac{1}{4} \min\left\{ \gamma^2\eta^2, 2\alpha\eta^2 \left(1 - \frac{\eta M_3}{\alpha}\right) \right\}.$$

For $t \in [t_i, t_i + \eta]$ then $\|c''(t)\| \in [\|c''(t_i)\| - \eta M_3, \|c''(t_i)\| + \eta M_3]$, so

$$\|c''(t_i)\| \left(1 - \frac{\eta M_3}{\alpha}\right) \leq \|c''(t)\| \leq \|c''(t_i)\| \left(1 + \frac{\eta M_3}{\alpha}\right).$$

This gives upper and lower estimates for the length of our cylinders within each η–interval. That is, choose h such that

$$\int_t^{t+h} \|c''(u)\|(t + h - u)\mathrm{d}u = \epsilon.$$

Then

$$\int_t^{t+h} \|c''(u)\|(t + h - u)\mathrm{d}u \leq \|c''(t_i)\|(1 + (\eta M_3/\alpha))(h^2/2).$$

Setting this equal to ϵ gives that

$$\|c''(t_i)\|(1 + (\eta M_3/\alpha))(h^2/2)) = \epsilon,$$

provided $h = \sqrt{2\epsilon}/\sqrt{\|c''(t_i)\|(1 + \eta M_3/\alpha)}$. The other estimate works in a similar fashion giving the bounds

$$h_{\min} := \frac{\sqrt{2\epsilon}}{\sqrt{\|c''(t_i)\|(1 + \frac{\eta M_3}{\alpha})}} \leq h \leq \frac{\sqrt{2\epsilon}}{\sqrt{\|c''(t_i)\|(1 - \frac{\eta M_3}{\alpha})}} =: h_{\max}.$$

Observe that $\eta < \alpha/M_3$, so that $(1 - (\eta M_3/\alpha)) > 0$. Further, note that

$$\epsilon < \frac{\eta^2(\alpha - \eta M_3))}{2},$$

ensuring that $h_{\max} < \eta$, so indeed there is at least one cylinder per η-interval.

Now let $N_i(\epsilon, c)$ be the number of cylinders contained completely within $[t_i, t_i + \eta]$ and $N(\epsilon, c)$ be the total number of cylinders produced by the algorithm.

Then since the cylinders may not fill up each η-interval, by counting $\sum_{i=1}^{\eta^{-1}} N_i(\epsilon, c)$ there are an additional η^{-1} many cylinders to consider. In the worst case,

$$\sqrt{\epsilon}N(\epsilon, c) \leq \sum_{i=0}^{\eta^{-1}} \sqrt{\epsilon}N_i(\epsilon, c) + \frac{\sqrt{\epsilon}}{\eta}.$$

Use the minimum length of a cylinder to conclude that

$$h_{\min}N_i(\epsilon, c) \leq \eta \Rightarrow \sqrt{\epsilon}N_i(\epsilon, c) \leq \eta\sqrt{\|c''(t_i)\|(1 + (\eta M_3/\alpha))}/\sqrt{2}.$$

This gives that

$$\sqrt{\epsilon}N(\epsilon, c) \leq \sum_{i=0}^{\eta^{-1}} \sqrt{\epsilon}N_i(\epsilon, c) + \frac{\sqrt{\epsilon}}{\eta} \leq \sum_{i=0}^{\eta^{-1}} \frac{\eta\sqrt{\|c''(t_i)\|(1 + \frac{\eta M_3}{\alpha})}}{\sqrt{2}} + \frac{\sqrt{\epsilon}}{\eta}.$$

Since $\epsilon < \gamma^2\eta^2/4$, it follows that $\sqrt{\epsilon}/\eta \leq \gamma/2$. Then the following holds:

$$\sqrt{\epsilon}N(\epsilon, c) \leq \sum_{i=1}^{\eta^{-1}} \sqrt{\epsilon}N_i(\epsilon, c) + \frac{\sqrt{\epsilon}}{\eta} \leq \nu + \frac{\gamma}{2} + \frac{\gamma}{2} = \nu + \gamma.$$

It remains to get a lower estimate for $N(\epsilon, c)$. The relation $\sum N_i(\epsilon, c) \leq N(\epsilon, c)$ holds by virtue that a tiny piece of each interval may have been missed. Now make sure that more cylinders can be inserted, that is, there are at least $h_{\max}N_i(\epsilon, c)$ space taken up in each η-interval. Then, it is true that $\eta - h_{\max}N_i(\epsilon, c) \leq h_{\min}$, otherwise $N_i(\epsilon, c)$ is not counted correctly. So this gives

$$\eta - \frac{\sqrt{2\epsilon}}{\sqrt{\|c''(t_i)\|(1 - \frac{\eta M_3}{\alpha})}} N_i(\epsilon, c) \leq \frac{\sqrt{2\epsilon}}{\sqrt{\|c''(t_i)\|(1 + \frac{\eta M_3}{\alpha})}}$$

or, equivalently,

$$\frac{\eta\sqrt{\|c''(t_i)\|(1 - \frac{\eta M_3}{\alpha})}}{2} - \sqrt{\epsilon}\sqrt{\frac{1 - \frac{\eta M_3}{\alpha}}{1 + \frac{\eta M_3}{\alpha}}} \leq \sqrt{\epsilon}N_i(\epsilon, c).$$

Since $\sqrt{(1-x)/(1+x)} \leq 1$ for $x > 0$ and $\sqrt{\epsilon}/\eta \leq \gamma/2$ and

$$\frac{\sqrt{\epsilon}}{\eta}\sqrt{\frac{1-(\eta M_3/\alpha)}{1+(\eta M_3/\alpha)}} \leq (\gamma/2).$$

Thus $-\gamma/2 \leq -(\sqrt{\epsilon}/\eta)\sqrt{(1-(\eta M_3/\alpha))/(1+(\eta M_3/\alpha))}$ and so summing yields

$$\begin{aligned}\nu - \gamma &\leq \nu - \frac{\gamma}{2} - \frac{\gamma}{2} \leq \frac{\eta\sqrt{\|c''(t_i)\|(1-\frac{\eta M_3}{\alpha})}}{2} - \frac{\sqrt{\epsilon}}{\eta}\sqrt{\frac{1-\frac{\eta M_3}{\alpha}}{1+\frac{\eta M_3}{\alpha}}} \\ &\leq \sum_{i=0}^{\eta^{-1}} \sqrt{\epsilon} N_i(\epsilon, c) \leq \sqrt{\epsilon} N(\epsilon, c).\end{aligned}$$

For the appropriate choices of η and ϵ, then $\nu - \gamma \leq \sqrt{\epsilon}N(\epsilon, c) \leq \nu + \gamma$ which gives the limit. □

If one continues to reduce the radii of the cylinders to be contained within the tubular neighborhood previously defined, then the result will be an adaptive, ambient isotopic PL approximation, requiring only technical modifications of arguments already published [32].

7. Visualization of molecular simulations with rich geometry

The techniques presented were motivated by applications for dynamic visualization in high performance computing (HPC) environments. A topologically complex geometric model is created to model the resting state of a macro-molecule. For chemical simulations of macro-molecules, the HPC algorithms will produce voluminous numerical data describing how the molecule twists and writhes under local chemical and kinetic changes. These are reflected in changed co-ordinates of the geometric model, namely perturbations of the kind discussed above. To produce a scientifically valid visualization, it is crucial that topological artifacts are not introduced by the visual approximations. Most past attention has focused only upon geometric approximations in each frame appropriate for efficient display. The proposed approach provides bounds for comparison with sufficient conditions to ensure that topological integrity is preserved.

Prototype animations have been implemented on both an open and closed curve. They are available for review over the web [35]. As previously mentioned in Section 6, ambient isotopy during animation of the PL approximations can be maintained in terms of the vertices of the PL approximation [7].

The sufficiency results in some conservatism — there may be perturbations beyond these limits that will still preserve ambient isotopy. However, that is very appropriate to this application. Namely, it now becomes easy to determine when the geometric perturbations approach an indicated limit, merely by a scalar comparison of the distance moved to the perturbation limit. This, alone, may be very valuable to the domain scientists, as this may indicate circumstances where the simulation should be investigated for critical changes. For instance, nearing this limit might signal a time just prior to fracture in a twisting DNA strand [10]. Furthermore, since this comparison is only between scalars, there may be overall performance gains relative to testing each frame for geometric self-intersections, because of the higher performance complexity of those geometric algorithms.

8. Conclusions and future work

Ambient isotopy is used as a crucial tool for modeling geometric changes at every instant within a time interval. Then ambient isotopic approximations can be created at any selected time within that interval. This reverses the standard animation approach of discretizing the time interval, creating an object at each time instant and then verifying the topology by checking whether new self-intersections may have occurred. Notably, if the time discretization had been badly chosen, then important topological changes could have been missed when the topological checking follows after the time discretization. The prior attention to topology eliminates that problem. Experimental opportunities remain to resolve pragmatic error bounds and HPC performance trade-offs.

Acknowledgements

The authors acknowledge, with appreciation, the many insightful and constructive comments of the anonymous reviewer.

Partial funding for Lance E. Miller was from NSF grant CCF 0429477 and from a 2006 IBM Doctoral Fellowship. All statements in this publication are the responsibility of the authors, not of these funding sources. Partial funding for E.L.F. Moore was from NSF grant CCF 0429477. Partial funding for T.J. Peters was from NSF grant CCF 0429477, from a 2005 IBM Faculty Award and from Kerner Graphics. Partial funding for A.C. Russell was from NSF grants CCF 0429477 and CCR 0226504.

References

[1] K. Abe, J. Bisceglio, D.R. Ferguson, T.J. Peters, A. Russell, T. Sakkalis, Computational topology for isotopic surface reconstruction, Theoretical Computer Science 365 (3) (2006) 184–198.
[2] K. Abe, J. Bisceglio, T.J. Peters, A.C. Russell, D.R. Ferguson, T. Sakkalis, Computational topology for reconstruction of surfaces with boundary: Integrating experiments and theory, in: M. Spagnuolo, A. Pasko, A. Belyaev (Eds.), International Conference of Shape Modeling and Applications, June 13–17, 2005, IEEE, IEEE Computer Society, Los Alamitos, CA, 2005, pp. 288–297.
[3] P. Agarwal, L. Guibas, A. Nguyen, D. Russel, L. Zhang, Collision detection for deforming necklaces, Computational Geometry: Theory and Applications 28 (2004) 137–163.
[4] P.K. Agarwal, H. Edelsbrunner, J. Harer, Y. Wang, Extreme elevation on a 2-manifold, in: SCG '04: Proceedings of the Twentieth Annual Symposium on Computational Geometry, ACM Press, New York, NY, USA, 2004, pp. 357–365.
[5] P.K. Agarwal, H. Edelsbrunner, Y. Wang, Computing the writhing number of a polygonal knot, in: SODA '02: Proceedings of the Thirteenth Annual ACM-SIAM Symposium on Discrete Algorithms, Society for Industrial and Applied Mathematics, Philadelphia, PA, USA, 2002, pp. 791–799.
[6] N. Amenta, T.J. Peters, A.C. Russell, Computational topology: ambient isotopic approximation of 2-manifolds, Theoretical Computer Science 305 (1–3) (2003) 3–15.
[7] L.-E. Andersson, S.M. Dorney, T.J. Peters, N.F. Stewart, Polyhedral perturbations that preserve topological form, Computer Aided Geometric Design 12 (1995) 785–799.
[8] L.-E. Andersson, T.J. Peters, N.F. Stewart, Selfintersection of composite curves and surfaces, Computer Aided Geometric Design 15 (5) (1998) 507–527.
[9] L.-E. Andersson, T.J. Peters, N.F. Stewart, Equivalence of topological form for curvilinear geometric objects, International Journal of Computational Geometry and Applications 10 (6) (2000) 609–622.
[10] E.D.T. Atkins, M.A. Taylor, Elongational flow studies on DNA in aqueous solution and stress-induced scission of the double helix, Biopolymers 32 (8) (1992) 911–923.
[11] R.C. Buck, Advanced Calculus, McGraw-Hill, New York, 1956.
[12] J. Cantarella, R.B. Kusner, J.M. Sullivan, On the minimum ropelength of knots and links, Inventiones Mathematica 150 (2) (2002) 257–286.
[13] J. Cantarella, M. Piatek, E. Rawdon, Visualizing the tightening of knots, in: VIS '05: Proceedings of the Conference on Visualization '05, IEEE Computer Society, Washington, DC, USA, 2005, pp. 575–582.
[14] K.L. Clarkson, Building triangulations using ϵ-nets, in: STOC '06: Proceedings of the Thirty-Eighth Annual ACM Symposium on Theory of Computing, ACM, New York, NY, USA, 2006, pp. 326–335.
[15] J.D. Cohen, M.C. Lin, D. Manocha, M.K. Ponamgi, I-COLLIDE: An interactive and exact collision detection system for large-scale environments, in: SI3D, vol. 218, 1995, pp. 189–196.
[16] L.H. de Figueiredo, J. Stolfi, L. Velho, Approximating parametric curves with strip trees using affine arithmetic, Computer Graphics Forum 22 (2) (2003) 171–180.
[17] H. Edelsbrunner, J. Harer, V. Natarajan, V. Pascucci, Morse-Smale complexes for piecewise linear 3-manifolds, in: SCG '03: Proceedings of the Nineteenth Annual Symposium on Computational Geometry, ACM Press, New York, NY, USA, 2003, pp. 361–370.
[18] H. Edelsbrunner, J. Harer, A. Zomorodian, Hierarchical Morse-Smale complexes for piecewise linear 2-manifolds, Discrete & Computational Geometry 30 (2003) 87–107.
[19] G. Farin, Curves and Surfaces for Computer Aided Geometric Design, 2nd edition, Academic Press, New York, NY, 1990.
[20] R. Fleischer, K. Mehlhorn, G. Rote, E. Welzl, C.-K. Yap, Simultaneous inner and outer approximation of shapes, Algorithmica 8 (5–6) (1992) 365–389.
[21] A. Gain, A. Dodgson, Preventing self-intersection under free-form deformation, IEEE Transactions on Visualization and Computer Graphics 7 (4) (2001) 289–298.
[22] S. Gottschalk, M.C. Lin, D. Manocha, Obbtree: A hierarchical structure for rapid interference detection, in: SIGGRAPH, 1996, pp. 171–180.
[23] N.K. Govindaraju, D. Knott, N. Jain, I. Kabul, R. Tamstorf, R. Gayle, M.C. Lin, D. Manocha, Interactive collision detection between deformable models using chromatic decomposition, ACM Transactions on Graphics 24 (3) (2005) 991–999.
[24] L. Guibas, Modeling motion, in: J. Goodman, J. O'Rourke (Eds.), Handbook of Discrete and Computational Geometry, 2nd edition, Chapman and Hall/CRC, 2004, pp. 1117–1134.
[25] S. Hadap, D. Eberle, P. Volino, M.C. Lin, S. Redon, C. Ericson, Collision detection and proximity queries, in: SIGGRAPH '04: ACM SIGGRAPH 2004 Course Notes, ACM Press, New York, NY, USA, 2004, p. 15.
[26] M.W. Hirsch, Differential Topology, Springer-Verlag, New York, 1976.
[27] J.G. Hocking, G.S. Young, Topology, Addison-Wesley, Reading, MA, 1961.
[28] H. Kim, L. Guibas, S. Shin, Efficient collision detection among moving spheres with unknown trajectories, Algorithmica 43 (3) (2005) 195–210.
[29] R. Kolodny, L. Guibas, M. Levitt, P. Koehl, Inverse kinematics in biology: The protein loop closure problem, Journal of Robotics Research 24 (2005) 151–162.
[30] R. Kopperman, M.B. Smyth, D. Spreen, J. Webster (Eds.), Spatial representation: discrete vs. continuous computational models, in: Dagstuhl Seminar Proceedings, vol. 04351, Internationales Begegnungs- und Forschungszentrum für Informatik (IBFI), Schloss Dagstuhl, Germany IBFI, Schloss Dagstuhl, Germany, 2005.
[31] J. Lasseter, Principles of traditional animation applied to 3D computer animation, SIGGRAPH Computer Graphics 21 (4) (1987) 35–44.
[32] T. Maekawa, N.M. Patrikalakis, T. Sakkalis, G. Yu, Analysis and applications of pipe surfaces, Computer Aided Geometric Design 15 (5) (1998) 437–458.
[33] L. Miller, E.L.F. Moore, T.J. Peters, A.C. Russell, Topological neighborhoods for spline curves: practice & theory, in: Lecture Notes in Computer Science, vol. 5045, 2008 (in press).
[34] E.L.F. Moore, Computational topology of spline curves for geometric and molecular approximations, Ph.D. Thesis, The University of Connecticut, 2006.
[35] E.L.F. Moore, T.J. Peters, Related topological animations, images and dissertation. Perturbing …. www.cse.uconn.edu/~tpeters.
[36] E.L.F. Moore, T.J. Peters, Computational topology for geometric design and molecular design, in: D.R. Ferguson, T.J. Peters (Eds.), Mathematics for Industry: Challenges and Frontiers: A Process View: Practice and Theory, Society for Industrial and Applied Mathematics, 2005, pp. 125–139.
[37] E.L.F. Moore, T.J. Peters, Floating point geometric algorithms for topologically correct scientific visualization. http://drops.dagstuhl.de/opus/volltexte/2006/717/, 2006.
[38] E.L.F. Moore, T.J. Peters, D.R. Ferguson, N.F. Stewart, Integrating topology and geometry for macro-molecular simulations, in: Kopperman et al. [30].
[39] E.L.F. Moore, T.J. Peters, J.A. Roulier, Preserving computational topology by subdivision of quadratic & cubic Bézier curves, Computing 79 (2007) 317–323.
[40] A. Pentland, J. Williams, Good vibrations: Model dynamics for graphics and animation, in: J.J. Thomas (Ed.), SIGGRAPH, ACM, 1989, pp. 215–222.
[41] T.J. Peters, J. Bisceglio, D.R. Ferguson, C.M. Hoffmann, T. Maekawa, N.M. Patrikalakis, T.T. Sakkalis, N.F. Stewart, Computational topology for regular closed sets (within the I-TANGO project), Topology Atlas 9 (1) (2004) 1–12.
[42] L. Piegl, W. Tiller, The NURBS Book, 2nd edition, Springer, New York, NY, 1997.
[43] C.R. Rourke, B.J. Sanderson, Introduction to Piecewise-Linear Topology, Springer-Verlag, New York, 1972.
[44] D. Russel, L. Guibas, Exploring protein folding conformations using spanners, in: Pacific Symposium on Biocomputing, 2005, pp. 40–51.
[45] T. Sakkalis, T.J. Peters, Ambient isotopic approximations for surface reconstruction and interval solids, in: Eighth ACM Symposium on Solid Modeling and Applications, ACM, June 2003, pp. 176–184.
[46] T. Sakkalis, T.J. Peters, J. Bisceglio, Isotopic approximations and interval solids, CAD 36 (11) (2004) 1089–1100.
[47] D.W.L. Sumners, Complexity measures for random knots, Computers & Chemistry 14 (4) (1990) 275–279.
[48] I.E. Sutherland, G.W. Hodgman, Reentrant polygon clipping, Communications of ACM 17 (1) (1974) 32–42.